A Compact Planar Wi-Fi Antenna with Optimized Radiation Patterns for Small UAV Applications

Ya-Lung Yang and Ding-Bing Lin *

Posted Date: 26 May 2023

doi: 10.20944/preprints202305.1723.v2

Keywords: planar Wi-Fi antenna; optimized radiation patterns; small UAV; unmanned aerial vehicle; vertically polarized radiation

Article

A Compact Planar Wi-Fi Antenna with Optimized Radiation Patterns for Small UAV Applications

Ya-Lung Yang and Ding-Bing Lin *

Department of Electronic and Computer Engineering, National Taiwan University of Science and Technology, Taipei 10607, Taiwan; d10602808@mail.ntust.edu.tw

* Correspondence: dblin@mail.ntust.edu.tw

Abstract: This paper proposes a compact planar Wi-Fi antenna with optimized radiation patterns for small unmanned aerial vehicle (UAV) applications in both urban and open areas. It is suitable for being mounted on the outermost side of the non-metallic wing of the small UAV. It has small dimensions of 16.5 mm (L) by 30.3 mm (W) by 1.6 mm (h), and the measured results of its prototype are in agreement with simulated data. Its impedance bandwidths over the two frequency ranges are 2.11 to 2.58 GHz and 5.06 to 7.5 GHz ($|S_{11}| \leq -10$ dB). At 5.8 GHz, it has stronger radiation below the small UAV to reduce interference from rare-use directions. Its maximum radiations, the directions of the maximum radiation in each elevation plane, are below the UAV and between 14 and 29 degrees from the horizontal plane. At 2.4 GHz, it has quasi-omnidirectional radiation to ensure a stable link in all directions, and its maximum radiations are near the horizontal plane. The optimized radiation patterns at 5.8 and 2.4 GHz can provide more antenna gain when the small UAV flies farther in urban and open areas, respectively. In addition, it has good vertically polarized radiation for long-distance applications.

Keywords: planar Wi-Fi antenna; optimized radiation patterns; small UAV; unmanned aerial vehicle; vertically polarized radiation

1. Introduction

With the rapid growth of the number of small unmanned aircraft vehicles (UAVs), their antenna design is becoming more and more important to ensure a stable link [1]. This study addresses an antenna design for light-and-small civil UAV applications in urban areas. Small UAVs tend to be light in weight and small in size for portability, so they are not suitable for mounting turntables or large phased-array antennas. Figure 1 shows the common scenarios of light-and-small civil UAV applications in urban areas, in which a person holding a remote control operates a quadcopter.

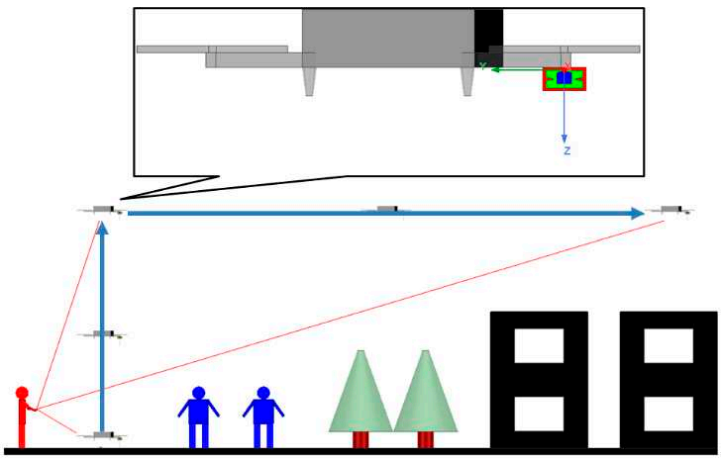

Figure 1. Common scenarios of light-and-small civil UAV applications in urban areas.

Peer-reviewed version available at Appl. Sci. 2023, 13, 7470; doi:https://doi.org/10.3390/app13137470

The proposed antenna is mounted below the propeller on the outermost side of the wing of a small UAV, away from large metal conductors such as printed circuit boards (PCBs) and batteries in the UAV body. The UAV takes off from the ground, flies vertically above ground objects, and then flies forward to the farthest position. The entire flight must avoid hitting ground objects such as people, trees, and buildings, so the UAV must keep flying higher than them. The distances between the UAV and the remote control are in order of taking off from the ground, flying vertically above ground objects, and flying forward to the farthest position.

For ensuring stable transmission quality and stability, the gain and polarization characteristics of the antenna are determined based on the Friis Transmission Equation [2]. The antenna must meet the following requirements to reduce interference and provide more antenna gain when the small UAV flies farther in urban areas. First, its $|S_{11}|$ must be equal to or smaller than -10 dB to ensure that the power can be delivered to the antenna efficiently. Second, it must have a small size and low profile to meet the portability and aerodynamic requirements for small UAV applications. Third, it must have stronger radiation below the UAV to reduce interference from rare-use directions. Because the UAV is always above the remote control as it flies away, it is farther away from the remote control than when it was just taking off. Fourth, its maximum radiations, the directions of the maximum radiation in each elevation plane, must be below the UAV and between 10 and 30 degrees from the horizontal plane to provide more antenna gain when the small UAV flies farther in urban areas. Finally, due to the boundary condition of the earth's ground plane, the antenna must have good vertically polarized radiation for long-distance applications.

Although many antenna architectures have been proposed [3–14] to meet the requirements for UAV applications, there is not yet a suitable one that can fully meet the requirements for small UAV applications in urban areas. Due to their small size and lightweight nature, folded dipole antennas have been proposed [3,4] for small and compact UAV applications, respectively. The fragmented antenna was proposed [3], and its overall dimensions and total mass are $0.96\,\lambda_0 \times 0.8\,\lambda_0 \times 0.8\,\lambda_0$ at 240 MHz and 18 g (including the matching circuit). A compact electrically tunable VHF antenna [4] was integrated into the landing gear of a compact UAV and has good vertically polarized radiation. However, neither of them has stronger radiation below the UAV, and their maximum radiations are near the horizontal plane. In addition, both of them need an extra matching circuit to match their characteristic impedance to 50 Ω for a better reflection coefficient at the operation frequency. The low-profile, quasi-omnidirectional Substrate Integrated Waveguide (SIW) Multihorn Antenna was proposed [5] for small nonmetallic UAV applications. It has good vertically polarized radiation and a low profile of 0.028 λ_0 at 2.4 GHz. However, it does not have stronger radiation below the UAV, and its lateral dimensions of $0.76\,\lambda_0 \times 0.76\,\lambda_0$ are too large for small UAVs. Due to their low profile and ability to conform to planar and nonplanar surfaces, patch antennas were proposed [6,7] for UAV applications. The high-gain dual-mode cylindrical conformal rectangular patch antenna [6] has a low profile of 0.508 mm (0.0175 λ_0 at 10.323 GHz), stronger radiation below the quadcopter UAV, and good vertically polarized radiation. The required radius of the arm of the UAV is 25 mm at the lowest operating frequency of 10.288 GHz, and it has to mount 3 patch antennas on the UAV arm to cover the hemisphere below the UAV. The conformal patch antennas [7] have a low profile of 3 mm (0.058 λ_0 at 5.8 GHz) and stronger radiation below the UAV. However, their maximum radiations are directly above each patch. Both of them proposed assembling multiple patch antennas on the UAV to ensure a stable link in the required directions. It takes up too much surface area, so they are not suitable for small UAVs. The design of a combined printed helical spiral antenna and helical inverted-F antenna [8] was miniaturized by co-winding the radiation elements on the same ceramic rod with a height of 24.7 mm (0.129 λ_0 at 1.57 GHz) and a radius of 6 mm. It was proposed for UAVs with global positioning system (GPS) L1 band and telemetry communication frequency band (2.33 GHz) applications. However, it does not have stronger radiation below the UAV at 2.33 GHz. The low-profile broadband plasma antenna [9] has different radiation patterns at different operating frequencies, and it also has a low profile of 0.105 λ_0 at 30 MHz. Its radiation pattern is omnidirectional at 30 MHz, and it has stronger radiation below the UAV at 300 and 500 MHz. However, it must be matched with an extra Butterworth low-pass filter and high-pass filter to isolate

Peer-reviewed version available at Appl. Sci. 2023, 13, 7470; doi:https://doi.org/10.3390/app13137470

the 13.56 MHz radio frequency signal that is used to activate plasma. Its complex structure and the need to use special materials such as plasma will result in a heavier weight and higher cost, so it is not suitable for small UAVs. The broadband slotted blade dipole antenna [10] has different radiation patterns at different operating frequencies. However, it must be matched with a special matching circuit, and it does not have stronger radiation below the UAV. In addition, its radiation patterns at all operating frequencies have nulls near the horizontal plane, which will cause the smallest gain when the UAV flies to the farthest position. Due to the advantages of its simple structure and low manufacturing cost using modern printed circuit technology, printed planar antennas were proposed [11–13] for UAV applications. The planar dual-mode dipole antenna [11] has a short electrical length of 0.3297 λ_0 at 0.86 GHz and good vertically polarized radiation. The omnidirectional vertically polarized antenna [12] also has good vertically polarized radiation, and it has different radiation patterns at different operating frequencies. However, neither of them has stronger radiation below the UAV, and their maximum radiations are near the horizontal plane. The wideband single-sided folded-off-center-fed dipole antenna [13] has good vertically polarized radiation and different radiation patterns at different operating frequencies. At 5 and 5.5 GHz, it has stronger radiation below the small UAV, and its maximum radiations are below the UAV and between 10 and 30 degrees from the horizontal plane. At 3.5 GHz, it has quasi-omnidirectional radiation, and its maximum radiations are near the horizontal plane. However, its electrical length of 0.469 λ_0 is too long for small UAV applications. A compact slot antenna with coplanar waveguide-fed [14] was not proposed for small UAV applications, and it has a very short electrical length of $0.16\,\lambda_0$ (L) and a low profile of $0.0128\,\lambda_0$ (h) to meet the portability and aerodynamic requirements for the small UAV applications. However, it does not have stronger radiation below the UAV, and its maximum radiations are near the horizontal plane.

Summarizing the above literature reviews, most proposed antennas have a radiation pattern with maximum radiations near the horizontal plane for UAV applications. This feature can meet the requirements for UAV applications in open areas and provide more antenna gain when the small UAV flies farther. The wideband single-sided folded-off-center-fed dipole antenna [13] is the best one; it has suitable radiation patterns to meet the requirements for small UAV applications in both urban and open areas. In addition, it also has the advantage of a simple and cost-efficient structure, which can make light-and-small civil UAVs more affordable. However, its electrical length of 0.469 λ_0 at 3.5 GHz is too long to meet the portability and aerodynamic requirements for small UAV applications.

Based on the structure with a short electrical length [14], this paper proposes a dual-band antenna with optimized radiation patterns for small UAV applications in both urban and open areas, respectively. It has a shorter electrical length of 0.132 λ_0 at 2.4 GHz than the best one that has been proposed [13]. First, this study considers that the small UAV has a camera function and needs to transmit real-time images to the remote control for the user to preview or store. To meet this application requirement, Wi-Fi 2.4 GHz and 5.8 GHz were selected as the operating frequencies. Secondly, since many technologies, such as Zigbee and Bluetooth, use 2.4 GHz as the operating frequency [15], there will be more interference at this frequency. Therefore, a quasi-directional radiation pattern was designed at 2.4 GHz, and its maximum radiations are near the horizontal plane for small UAV applications in open areas with less interference, such as mountains, oceans, or farmland. Third, an end-fire radiation pattern was designed at 5.8 GHz for small UAV applications in urban areas. It has stronger radiation below the UAV, and its maximum radiations are below the UAV and between 14 and 29 degrees from the horizontal plane. Finally, to ensure that the characteristics of this antenna will not be significantly affected when it is applied to small UAVs, the following assumptions are made in this study: First, as shown in Figure 1, the objects around the antenna, such as the UAV wing and propeller, must be made of non-metallic material. Second, the large metal conductors like PCBs and batteries in the UAV body must be located in the far-field region of the proposed antenna. Based on the definition of the far-field region [16], the distance between the small UAV body and the proposed antenna must be more than 46 mm.

Peer-reviewed version available at Appl. Sci. 2023, 13, 7470; doi:https://doi.org/10.3390/app13137470

By performing the theoretical analysis, full-wave simulation, and prototype measurement, we verified that the proposed antenna can meet the requirements for light-and-small civil UAV applications in both urban and open areas. The rest of this paper is as follows: Section II presents the antenna design methodology, which includes the proposed antenna's structural topology and theoretical analysis. Section III presents the full-wave simulations for validating the design theory. Section IV presents the antenna prototype, the measurement setup, the comparisons of the simulated data and measured results of the prototype, and discussions about the results. Finally, Section V summarizes the results and future work.

2. Antenna Design and Analysis

In this study, a compact slot antenna with coplanar waveguide (CPW)-fed was designed that supports Wi-Fi dual-band communication and has a single-sided planar structure.

2.1. Antenna Structure

Figure 2 shows the configuration of the proposed antenna. At 5.8 GHz, the four corners of its outer conductor are the main radiation sources, forming end-fire radiation. At 2.4 GHz, the two sides of the outer conductor are the main effective radiation sources, forming quasi-omnidirectional radiation.

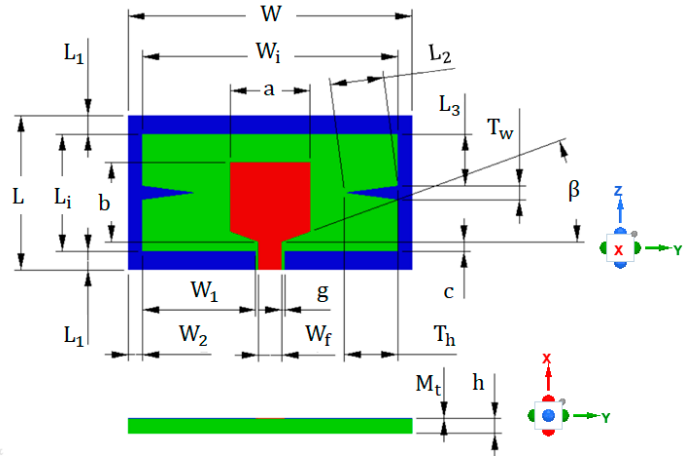

Figure 2. Configuration of the proposed antenna.

Table 1 displays the values of geometrical parameters for the proposed antenna. The thickness of the metal layer (M_t) is 0.035 mm, of which 0.031 mm is copper, 0.003 mm is nickel, and 0.001 mm is gold. It was printed on the FR4 substrate with a relative permittivity of 4.4, a loss tangent of 0.02, a thickness of 1.6 mm (h), and planar dimensions of 16.5 mm (L) by 30.3 mm (W). At the fed port, the width of the central conducting track (W_f) is 2.5 mm, and a pair of outer conducting tracks are separated from the central conducting track by a small gap (g) of 0.3 mm to achieve a characteristic impedance of 50 Ω. The antenna is symmetrical on both sides of the x-z plane, so the radiation generated by the current components in the +y and -y directions will cancel each other out. Therefore, the currents in the +z and -z directions are the main radiation sources, making this antenna have good vertically polarized radiation.

Table 1. The values of geometrical parameters for the proposed antenna.

Parameter	Dimension (mm)	Wavelength of 2.4 GHz in vacuum	Wavelength of 5.8 GHz in vacuum	Angle (degree)
W	30.3	0.24	0.59	
W_i	27.3	0.22	0.53	
L	16.5	0.13	0.32	

L_i	12.5	0.10	0.24	
W_1	12.1	0.10	0.23	
W_2	1.5	0.01	0.03	
L_1	2	0.02	0.04	
L_2	5.75	0.05	0.11	
L_3	5.5	0.04	0.11	
a	8.5	0.07	0.16	
b	8.5	0.07	0.16	
c	1	0.01	0.02	
T_h	5.7	0.05	0.11	
T_w	1.5	0.01	0.03	
W_f	2.5	0.02	0.05	
g	0.3	0.00	0.01	
C_t	0.035	0.00	0.00	
h	1.6	0.01	0.03	
β				20

2.2. Antenna Design for 5.8 GHz

Figure 3 shows the simulated surface current density at 5.8 GHz, where the areas with higher surface current densities are the main radiation areas. The outer conductor forms four monopole antennas from each triangle vertex to its two adjacent corners. These four monopoles have the same wavelength, λ_H, and the upper resonance frequency, f_H, can be approximated by using (1), where c is the speed of light in vacuum (3×10^8 m/s).

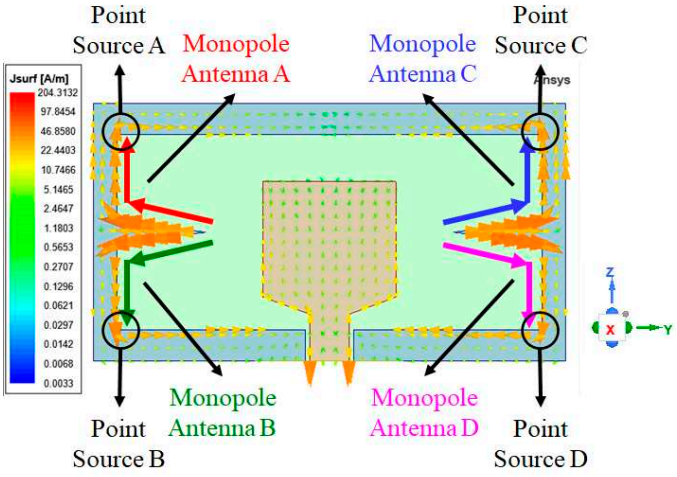

Figure 3. The simulated surface current density at 5.8 GHz.

$$f_H \cong \frac{c}{\lambda_H} = \frac{c}{(L_2+L_3+L_1/2)/0.23} = 5.63 \text{ GHz}, \quad (1)$$

There are higher surface current densities at the four corners inside the outer conductor, which approximate four point-sources, named Element A, Element B, Element C, and Element D. The radiation pattern is mainly synthesized from these four point-sources. Because of the electric field that radiates between the inner and outer conductors, the proposed antenna approximates a two-element array of two point-sources, Element 1 and 2, as shown in Figure 4.

Peer-reviewed version available at Appl. Sci. 2023, 13, 7470; doi:https://doi.org/10.3390/app13137470

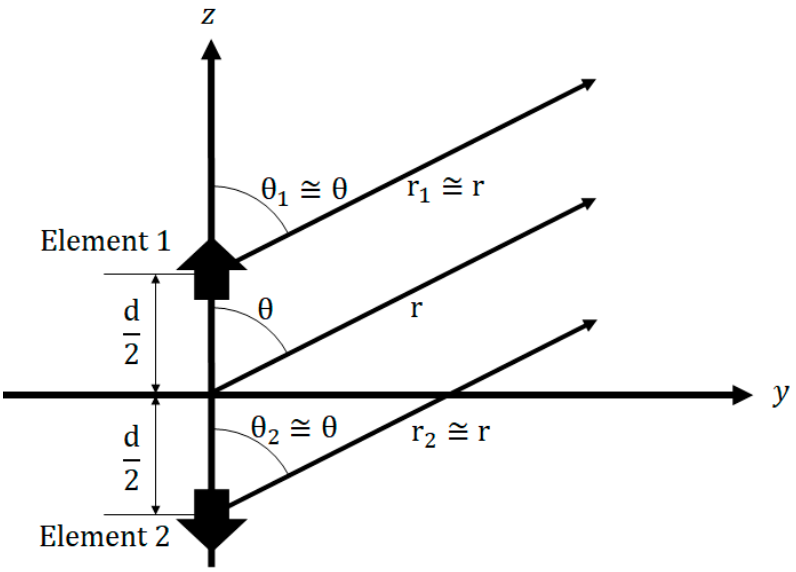

Figure 4. Far-field observation of a two-element array consisting of two point- sources, Element 1 and 2, positioned along the z-axis.

Where the radiation patterns of Elements 1 and 2 are equal to the sum of Elements A and C and the sum of Elements B and D, respectively. Furthermore, since the cross-sectional area of the inner conductor used as the reference plane is very small, the radiation patterns of both Element 1 and 2 approximate a vertical infinitesimal dipole. Based on the directivity of the vertical infinitesimal (Hertzian) dipole [17], the normalized pattern function of the vertical infinitesimal dipole is $\sin^2\theta$. The normalized array factor of Element 1 and 2 is adapted from (2) [18]. Where k is the wave number equal to $2\pi/\lambda_{5.8G}$, and d is the distance between Element 1 and 2, approximately equal to $L_i + (L_1/2) \times 2$.

$$(AF_{12})_n = \cos\left[\frac{1}{2}(kd\cos\theta + \beta_d)\right] = \cos\left\{\frac{1}{2}\left[\frac{2\pi}{\lambda_{5.8G}}(L_i + (L_1/2) \times 2)\cos\theta + \beta_d\right]\right\} = \cos\left[\frac{1}{2}(100.92^\circ \times \cos\theta + \beta_d)\right], \quad (2)$$

At 5.8 GHz, the difference in phase excitation, $\beta_d = \beta_A - \beta_B = \beta_C - \beta_D$, can be derived by (3). Where β_A, β_B, β_C, and β_D are the phase excitations of the Element A, B, C, and D, respectively. In addition, β_A is equal to β_C, and the negative sign indicates the phase lag.

$$\beta_d = -\frac{2\times\pi}{\lambda_{5.8G}} \times (L_i + (L_1/2) \times 2 - T_w) = -90.48^\circ, \quad (3)$$

In (2), replace β_d with -90.48°, the normalized array factor of Element 1 and 2 can be written as (4). It has two maximums at $\theta = +26°$ and $\theta = -26°$ and only one minimum at $\theta = +180°$, and it forms an end-fire array toward $0°$.

$$(AF_{12})_n = \cos\left[\frac{1}{2}(100.92^\circ \times \cos\theta - 90.48^\circ)\right], \quad (4)$$

The normalized total field of the two-element array antenna is written as (5). It has two maximums at $\theta = +60°$ and $\theta = -60°$ and only one minimum at $\theta = +180°$, and it forms an end-fire radiation toward $0°$.

$$(E_{total})_n = \{\sin^2\theta \times (AF_{12})_n\}_n, \quad (5)$$

Figure 5 shows the relative power patterns of the vertical infinitesimal dipole, the array factor of Element 1 and 2, and the total field of the two-element array antenna.

Peer-reviewed version available at Appl. Sci. 2023, 13, 7470; doi:https://doi.org/10.3390/app13137470

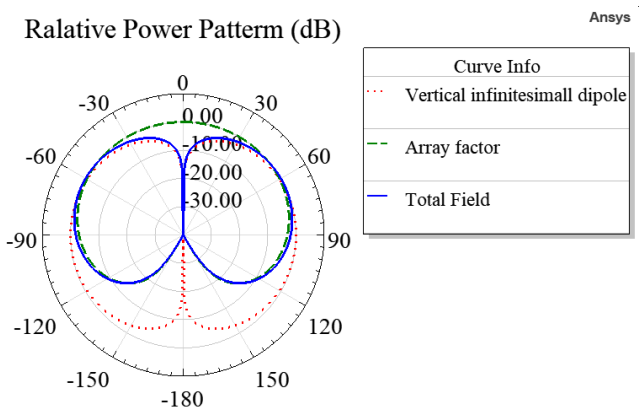

Figure 5. The relative power patterns of the vertical infinitesimal dipole, the array factor of Element 1 and 2, and the total field of the two-element array antenna.

2.3. Antenna Design for 2.4 GHz

Figure 6 shows the simulated surface current densities at 2.4 GHz, where the areas with higher surface current densities are the main radiation areas. The two sides of the outer conductor form a pair of L-shaped monopoles, Monopole E and Monopole F. These two monopoles have the same wavelength, λ_L, and the lower resonance frequency, f_L, can be approximated by using (6).

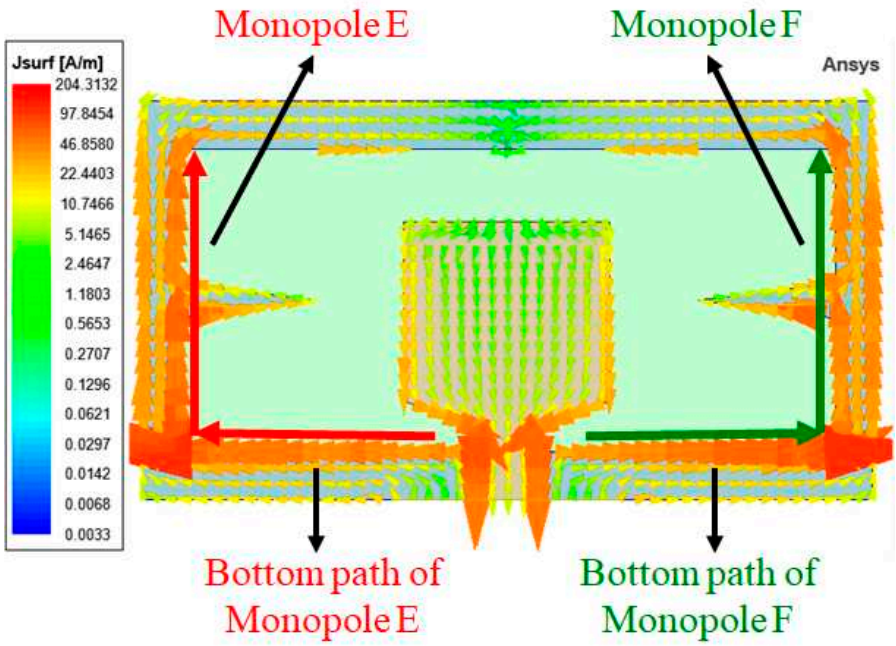

Figure 6. The simulated surface current density at 2.4 GHz.

$$f_L \cong \frac{c}{\lambda_L} = \frac{c}{\{[W_1+(W_2/2)]+[L_i+(L_1/2)\times 2]\}/0.23} = 2.52 \text{ GHz}, \quad (6)$$

Due to the symmetrical design of the architecture, the radiations from the two bottom paths will cancel each other out. Because of the electric field that radiates between the inner and outer conductors, the proposed antenna approximates a vertical monopole antenna. In addition, since the cross-sectional area of the inner conductor used as the reference plane is very small, the radiation pattern of the vertical monopole antenna approximates that of a vertical dipole with an effective length of $L_i + (L_1/2) \times 2$, equivalent to 0.122 λ_L. Its maximum radiations are near the horizontal plane.

3. Full-Wave Simulation

Peer-reviewed version available at Appl. Sci. 2023, 13, 7470; doi:https://doi.org/10.3390/app13137470

The proposed antenna was simulated by the ANSYS High-Frequency Structure Simulator (HFSS) [19]. From (1), f_H decreases as L_2 increases, and L_2 can be derived from (7), L_2 increases as T_h increases. Hence, f_H decreases as T_h increases.

$$L_2 = \sqrt{{T_h}^2 + \left(\frac{T_w}{2}\right)^2} = \sqrt{5.7^2 + \left(\frac{1.5}{2}\right)^2} = 5.75, \quad (7)$$

Figure 7 shows the simulated reflection coefficients for different values of T_h. The simulated data are in agreement with (1) and (7), f_H decreases as T_h increases, and f_H is about 5.63 GHz when T_h is equal to 5.7 mm.

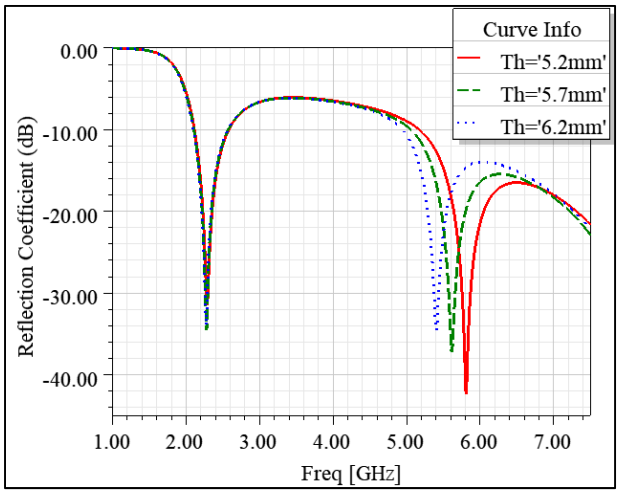

Figure 7. The simulated reflection coefficients for different values of T_h.

From (6), f_L decreases as W_1 increases, and Figure 8 shows the simulated reflection coefficients for different values of W_1. The simulated data are in agreement with (6), f_L decreases as W_1 increases.

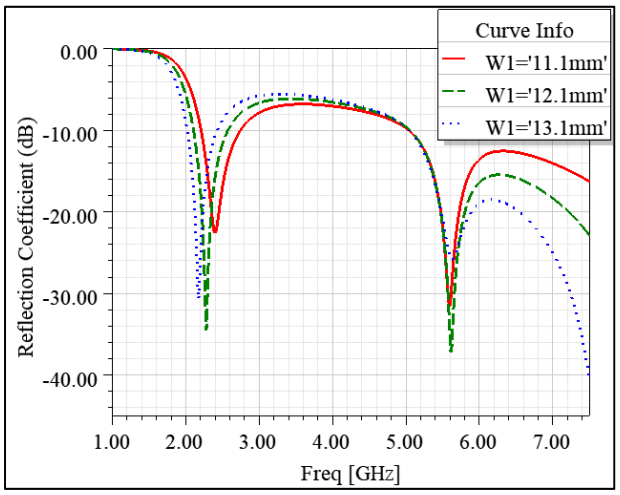

Figure 8. The simulated reflection coefficients for different values of W_1.

From (2) and (5), the normalized total field at 5.8 GHz changes as β_d changes, and from (3), β_d gets closer to -100.92° as T_w decreases closer to zero. Hence, the end-fire radiation becomes more significant as T_w decreases. Figure 9 shows the simulated radiation patterns at 5.8 GHz in the y-z plane for different values of T_w. The simulated data are in agreement with (2), (3), and (5), and the end-fire radiation becomes more significant as T_w decreases.

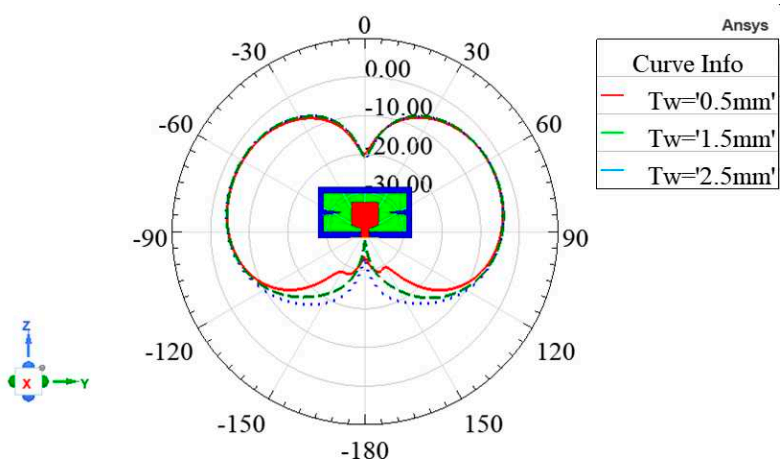

Figure 9. The simulated radiation patterns at 5.8 GHz in the y-z plane for different values of T_w.

4. The Comparisons of Simulated Data and Measured Results of The Prototype

Figure 10 shows the prototype of the proposed antenna with an SMA connector [20] soldered to it, where the hand-soldered tin had not been incorporated in the simulation. The antenna had been measured by the Atenlab A3 compact type OTA measurement system [21] and compared with its simulated data.

Figure 10. The prototype of the proposed antenna with an SMA connector soldered to it.

Figure 11(a), (b), and (c) show the measurement setup for radiation patterns in the x-y, x-z, and y-z planes, respectively. The proposed antenna was placed on a turntable and connected to the coaxial cable of the measurement system which had not been incorporated in the simulation. Figure 11(a) shows the proposed antenna was connected directly to the coaxial cable of the measurement system, and the cable was parallel to the z-axis of the proposed antenna. Figure 11(b) and (c) show the proposed antennas were connected to the coaxial cable of the measurement system via a right-angle SMA adapter [22], and the cable was perpendicular to the z-axis of the proposed antennas.

Peer-reviewed version available at Appl. Sci. 2023, 13, 7470; doi:https://doi.org/10.3390/app13137470

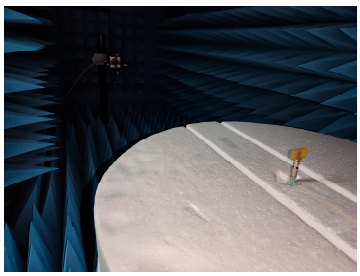

(**a**)

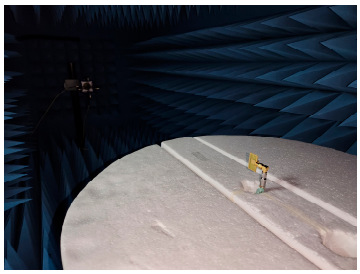

(b)

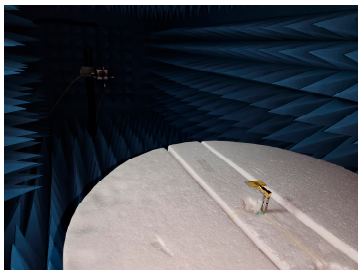

(c)

Figure 11. The measurement setup for radiation patterns. (**a**) x-y plane; (**b**) x-y plane; (**c**) x-y plane.

4.1. Reflection Coefficients

Figure 12 shows the comparison of the simulated and measured reflection coefficients of the proposed antenna. The simulated curve shows that the proposed antenna can meet $|S_{11}| \leq -10$ dB from 2.11 to 2.58 GHz and from 5.06 to 7.5 GHz, where the fractional bandwidths are 20.04 % and 38.05 %, respectively. The measured result is in agreement with the simulated one, and it can meet Wi-Fi 2.4 and 5.8 GHz requirements for small UAV applications.

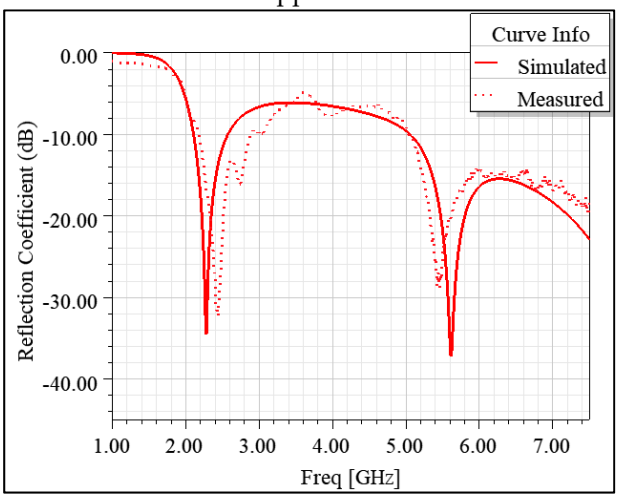

Figure 12. The comparison of the simulated and measured reflection coefficients of the proposed antenna.

4.2. Radiation Patterns

Figures 13, 14, and 15 show the comparisons of the simulated and measured radiation patterns of the proposed antenna in the x-y, x-z, and y-z planes, respectively. The simulated data show the proposed antenna has good vertically polarized radiation. Figure 13(a) and (b) show the radiation patterns of the proposed antenna in the x-y plane at 2.4 and 5.8 GHz, respectively, and the vertically polarized radiations are quasi-omnidirectional. Due to the hand-soldered tins on the main radiation areas of 2.4 GHz, the measured horizontally polarized radiation is larger than the simulated one, as shown in Figure 13(a).

Peer-reviewed version available at Appl. Sci. 2023, 13, 7470; doi:https://doi.org/10.3390/app13137470

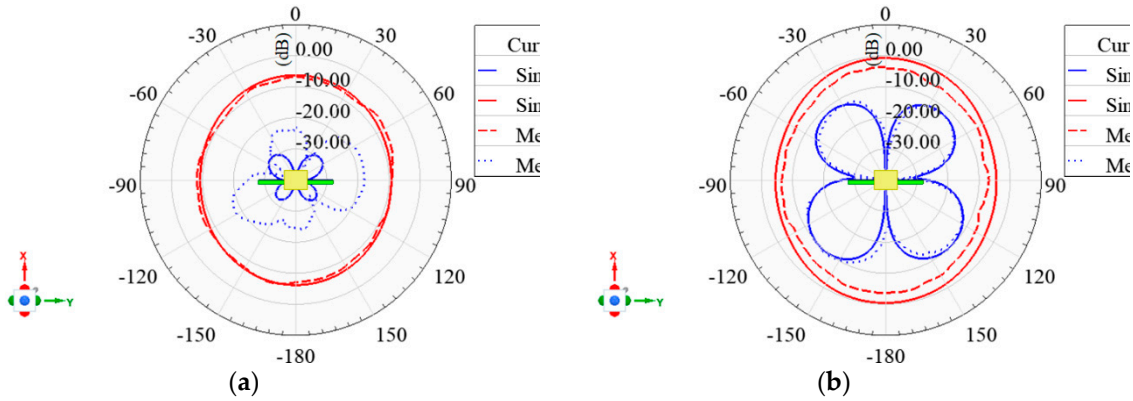

Figure 13. The comparison of the simulated and measured radiation patterns of the proposed antenna in the x-y plane. (**a**) 2.4 GHz; (**b**) 5.8 GHz.

In the x-z and y-z planes, due to the cable effect, the measured horizontally polarized radiations are much larger than the simulated data, as shown in Figure 14 and 15. In addition, due to the cable effect, the measured vertically polarized radiation is larger than the simulated one at −120° to +120° in the y-z plane at 5.8 GHz, as shown in Figure 15(b).

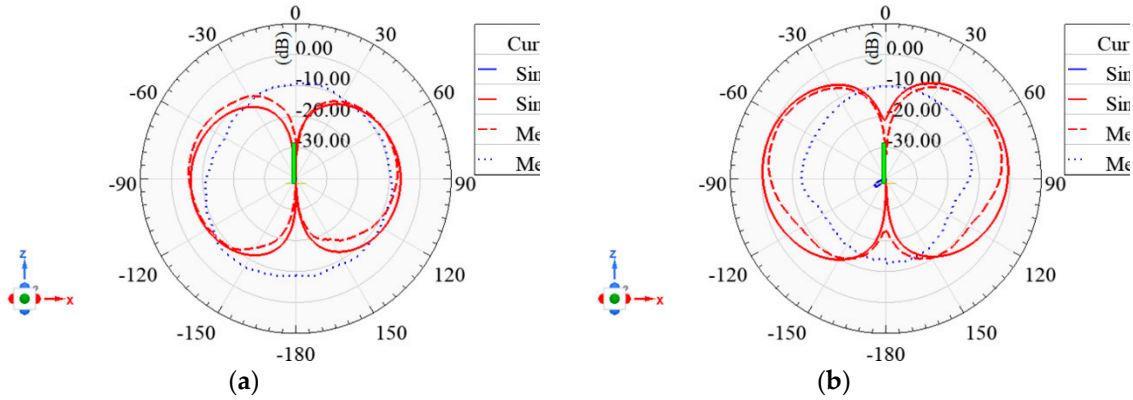

Figure 14. The comparison of the simulated and measured radiation patterns of the proposed antenna in the x-z plane. (**a**) 2.4 GHz; (**b**) 5.8 GHz.

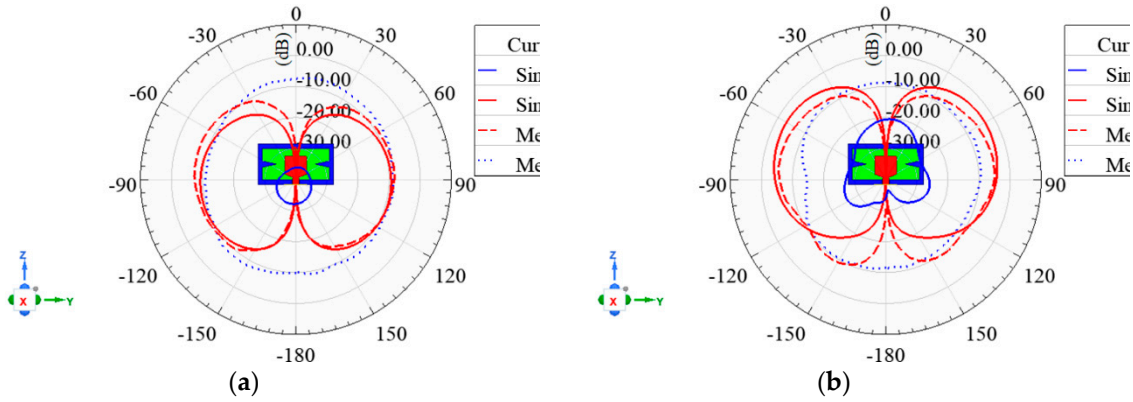

Figure 15. The comparison of the simulated and measured radiation patterns of the proposed antenna in the y-z plane. (a) 2.4 GHz; (b) 5.8 GHz.

The simulated vertically polarized radiation patterns at 2.4 GHz are quasi-omnidirectional, and the maximum radiations in the x-z and y-z planes are near the horizontal plane, as shown in Figure 13(a), 14(a), and 15(a). The simulated vertically polarized radiation patterns at 5.8 GHz have stronger radiation in the upper hemisphere (below the UAV), as shown in Figure 14(b) and 15(b). Its maximum

Peer-reviewed version available at Appl. Sci. 2023, 13, 7470; doi:https://doi.org/10.3390/app13137470

radiations in the x-z and y-z planes are in the upper hemisphere and between 14 and 29 degrees from the horizontal plane.

Table 2 displays the characteristics of the simulated vertically polarized radiation patterns. Ignoring the influence caused by the hand-soldered tin and the cable effect of the measurement system, all measured results of radiation patterns are in agreement with simulated data. In E-planes, the beamwidths of relative -10 dB at 2.4 GHz are no less than 142 degrees. Moreover, at 5.8 GHz, maximum gain angles are between 17 and 29 degrees off the horizontal.

Table 2. The Characteristics of the Simulated Vertically Polarized Radiation Patterns.

Unit: degree			y-z plane				x-z plane			
			Left plane		Right plane		Left plane		Right plane	
2.4 GHz	Maximum gain angle		-98		98		-95		91	
	Relative -3 dB	Beam angle	-142	-49	48	142	-139	-49	46	134
		Beamwidth	93		94		90		88	
	Relative -10 dB	Beam angle	-165	-20	19	165	-165	-21	18	160
		Beamwidth	145		146		144		142	
5.8 GHz	Maximum gain angle		-61		62		-76		73	
	Relative -3 dB	Beam angle	-102	-29	29	103	-118	-39	37	114
		Beamwidth	72.96		74		79		77	
	Relative -10 dB	Beam angle	-127	-11	11	129	-152	-16	14	148
		Beamwidth	116		118		136		134	

Table 3 displays the comparison of the proposed antenna and published works on planar antennas. The proposed planar antenna has the following advantages. First, it has a single-sided structure, which has a relatively low cost to make small UAVs more affordable. Second, it has a minimum electrical length (L) of 0.132 λ_0 and a low profile (h) of 0.0128 λ_0 to meet the portability and aerodynamic requirements for small UAV applications. Third, at 5.8 GHz, it has stronger radiation in the upper hemisphere (below the small UAV) to reduce interference from rare-use directions. Its maximum radiations are below the UAV and between 14 and 29 degrees from the horizontal plane to provide more antenna gain when the small UAV flies farther in urban areas. At 2.4 GHz, it has quasi-omnidirectional radiation to ensure a stable link in all directions. Its maximum radiations are near the horizontal plane to provide more antenna gain when the small UAV flies farther in open areas. Finally, it has good vertically polarized radiation at both 2.4 and 5.8 GHz for long-distance applications.

Table 3. The comparison of the proposed antenna ad published works on planar antennas.

Ref.	Structure	Operating Frequency	Radiation Pattern		Electrical Dimensions (L × W × h) (λ_0)
			For Urban Areas	For Open Areas	
[11]	Double-sided	0.86 to 1.51		Yes	0.3297 × 0.0344 × 0.0046
[12]	Double-sided	3.9 to 5		Yes	2.3400 × 0.1820 × 0.0260
[13]	Single-sided	3.5/3.7/4.5/5/5.7	Yes	Yes	0.4690 × 0.1470 × 0.0092
[14]	Single-sided	2.4 to 5.8		Yes	0.1600 × 0.2000 × 0.0128
This work	Single-sided	2.4/5.8	Yes	Yes	0.1320 × 0.2424 × 0.0128

5. Conclusions

Peer-reviewed version available at *Appl. Sci.* **2023**, *13*, 7470; doi:https://doi.org/10.3390/app13137470

In summary, we report a compact planar Wi-Fi antenna with optimized radiation patterns for small UAV applications in urban and open areas, respectively. The proposed antenna had been prototyped and measured, and the measured results are in agreement with the simulated data. It has end-fire radiation to reduce the interference from rare-use directions at 5.8 GHz and quasi-omnidirectional radiation to ensure a stable link in all directions at 2.4 GHz. The directions of the maximum radiation in each elevation plane at 5.8 and 2.4 GHz provide more antenna gain when the small UAV flies farther in urban and open areas, respectively. In future work, the proposed antenna will be mounted on a small UAV for field experiments.

References

1. C. Xu, X. Liao, J. Tan, H. Ye and H. Lu, "Recent Research Progress of Unmanned Aerial Vehicle Regulation Policies and Technologies in Urban Low Altitude," in *IEEE Access*, vol. 8, pp. 74175-74194, 2020, doi: 10.1109/ACCESS.2020.2987622.
2. C. A. Balanis, "Antenna Theory: Analysis and Design," 4th ed., New York, NY, USA: Wiley, 2016, ch. 2, sec. 17, pp. 89.
3. N. Barani, J. F. Harvey and K. Sarabandi, "Fragmented Antenna Realization Using Coupled Small Radiating Elements," in *IEEE Transactions on Antennas and Propagation*, vol. 66, no. 4, pp. 1725-1735, April 2018, doi: 10.1109/TAP.2018.2806397.
4. C. Pfeiffer and F. T. Dagefu, "A Compact Electrically Tunable VHF Antenna," *2019 IEEE International Symposium on Antennas and Propagation and USNC-URSI Radio Science Meeting*, Atlanta, GA, USA, 2019, pp. 1549-1550, doi: 10.1109/APUSNCURSINRSM.2019.8889368.
5. L. Sun, B. Sun, J. Yuan, W. Tang and H. Wu, "Low-Profile, Quasi-Omnidirectional Substrate Integrated Waveguide (SIW) Multihorn Antenna," in *IEEE Antennas and Wireless Propagation Letters*, vol. 15, pp. 818-821, 2016, doi: 10.1109/LAWP.2015.2476346.
6. S. Pradhan and B. Gupta, "High-Gain Dual-Mode Cylindrical Rectangular Patch Antenna for Airborne Applications," in *IEEE Transactions on Aerospace and Electronic Systems*, vol. 58, no. 5, pp. 4168-4179, Oct. 2022, doi: 10.1109/TAES.2022.3161611.
7. A. V. Durán-Pardo, D. V. Navarro-Méndez, L. F. Carrera-Suárez and M. Baquero-Escudero, "Conformal Patch Antennas for an UAV employed in Agricultural Applications," *2020 IEEE International Symposium on Antennas and Propagation and North American Radio Science Meeting*, Montreal, QC, Canada, 2020, pp. 285-286, doi: 10.1109/IEEECONF35879.2020.9330115.
8. Y. Han *et al*., "Design of Combined Printed Helical Spiral Antenna and Helical Inverted-F Antenna for Unmanned Aerial Vehicle Application," in *IEEE Access*, vol. 8, pp. 54115-54124, 2020, doi: 10.1109/ACCESS.2020.2981041.
9. C. Wang, B. Yuan, W. Shi and J. Mao, "Low-Profile Broadband Plasma Antenna for Naval Communications in VHF and UHF Bands," in *IEEE Transactions on Antennas and Propagation*, vol. 68, no. 6, pp. 4271-4282, June 2020, doi: 10.1109/TAP.2020.2972397.
10. M. Nosrati, A. Jafargholi, R. Pazoki and N. Tavassolian, "Broadband Slotted Blade Dipole Antenna for Airborne UAV Applications," in *IEEE Transactions on Antennas and Propagation*, vol. 66, no. 8, pp. 3857-3864, Aug. 2018, doi: 10.1109/TAP.2018.2835524.
11. H. -T. Chou, D. -B. Lin and H. -L. Chiu, "Planar Dual-Mode Dipole Antenna Formed by Artificial Microstrip Arms Loaded With Multiple H-Slots for Broadband Operation of Vertically Polarized Radiation on UAV Platform," in *IEEE Transactions on Antennas and Propagation*, vol. 70, no. 9, pp. 7869-7877, Sept. 2022, doi: 10.1109/TAP.2022.3177535.
12. Y. -D. Yan and Y. -C. Jiao, "Omnidirection Vertically Polarized Antenna on Unmanned Aerial Vehicle," *2018 12th International Symposium on Antennas, Propagation and EM Theory (ISAPE)*, Hangzhou, China, 2018, pp. 1-3, doi: 10.1109/ISAPE.2018.8634378.
13. M. Sumi and Y. Suzuki, "A Wideband Single-Sided Folded-Off-Center-Fed Dipole Antenna for 4G/5G/Wi-Fi M2M/IoT Applications and UAVs," *2021 IEEE Conference on Antenna Measurements & Applications (CAMA)*, Antibes Juan-les-Pins, France, 2021, pp. 3-4, doi: 10.1109/CAMA49227.2021.9703546.
14. D. -B. Lin, I. -T. Tang, Y. -J. Wei and H. -P. Lin, "A compact slot antenna with CPW-fed for IEEE 802.16-2004 applications," *2007 IEEE Antennas and Propagation Society International Symposium*, Honolulu, HI, USA, 2007, pp. 4753-4756, doi: 10.1109/APS.2007.4396606.
15. P. K. Reddy Maddikunta *et al*., "Unmanned Aerial Vehicles in Smart Agriculture: Applications, Requirements, and Challenges," in *IEEE Sensors Journal*, vol. 21, no. 16, pp. 17608-17619, 15 Aug.15, 2021, doi: 10.1109/JSEN.2021.3049471.
16. "IEEE Standard for Definitions of Terms for Antennas," in *IEEE Std 145-2013 (Revision of IEEE Std 145-1993)* , vol., no., pp.1-50, 6 March 2014, doi: 10.1109/IEEESTD.2014.6758443.

17. David K. Cheng, '" Fundamentals of Engineering Electromagnetics," Menlo Park, CA, USA: Addison-Wesley, 1993, ch. 10, sec. 3, pp. 432–433.
18. C. A. Balanis, "Antenna Theory: Analysis and Design," 4th ed., New York, NY, USA: Wiley, 2016, ch. 6, sec. 2, pp. 287.
19. ANSYS Incorporation, High-Frequency Structure Simulator (HFSS), Version 2022 R1, Nov. 7. 2022. [Online]. Available: https://www.ansys.com/products/electronics/ansys-hfss
20. SMA PCB End Launch Straight Jack 50 Ohm, Amphenol Corporation, Jan. 2023. https://www.amphenolrf.com/901-10309.html
21. Atenlab A3 Measurement System, PCB GraphTech Pte, Nov. 2022. https://pcbgt.com.sg/atenlab-a3
22. SMA Jack to SMA Plug Adapter 50 Ohm Right Angle, Amphenol Corporation, Jan. 2023. https://www.amphenolrf.com/132172.html